RSC Advances

PAPER

View Article Online
View Journal | View Issue

Cite this: *RSC Adv.*, 2017, **7**, 16238

Enhanced removal of Cd(II) from aqueous solution using $CaCO_3$ nanoparticle modified sewage sludge biochar†

Wei-Qi Zuo,[ab] Chen Chen,[ab] Hao-Jie Cui*[ab] and Ming-Lai Fu*[ab]

Received 9th January 2017
Accepted 7th March 2017

DOI: 10.1039/c7ra00324b

rsc.li/rsc-advances

Nanostructured $CaCO_3$ modified sewage sludge biochar (CMSSB) was successfully fabricated for efficient removal of Cd(II) from aqueous solutions. X-ray diffraction (XRD) and scanning electron microscopy (SEM) analyses indicated that the loaded $CaCO_3$ mainly existed in the form of dispersive calcite nanoparticles, and the loading of calcite nanoparticles had a slight effect on the morphology of the sewage sludge biochar (SSB). The adsorption capacity of the obtained CMSSB for Cd(II) based on the Langmuir model is 36.5 mg g^{-1}, which was nearly three times higher than that of the pristine SSB. The adsorption process can be well described by the Elovich model, and the initial adsorption rate of the CMSSB is faster than that of the SSB. The Cd(II) adsorption mechanism on the CMSSB involves ion-exchange and precipitation reactions between heavy metal ions and calcite nanoparticles and biochar. The present results suggested that the as-prepared CMSSB is an efficient and economic adsorbent for environmental heavy metal remediation.

Introduction

Cadmium (Cd) contaminant in water and soils has attracted much attention because it poses a serious threat to human health.[1,2] Various remediation technologies have been used for Cd(II) decontamination of polluted water and soils, including but not limited to chemical precipitation, membrane filtration, ion-exchange, adsorption, solidification, and electrochemical methods.[3,4] Among these technologies, adsorption is the most used method because of its flexibility in design and operation. Economy, efficiency, and being green are three key factors to be considered in polluted water and soil treatment. Thus, it is very desirable to prepare a low-cost, high efficiency, and environmentally friendly adsorbent for environmental applications.

On the other hand, the disposal and utilization of municipal sewage sludge (SS) are a growing concern due to the rapid increase in amounts of wastewater treatment plants in China. In recent years, carbonization, a pyrolysis process that mostly leaves a char product, has been explored extensively as an alternative method for SS treatment and it is a promising technology to recover nutrients from SS, kill pathogens and concentrate heavy metals simultaneously.[5] Meanwhile, biochar, including biochar produced from sewage sludge, has been widely used to wastewater treatment and soil amendment.[6–10] The development of biochar technology provides opportunities to satisfy the need of low-cost adsorbents for aqueous heavy metals.[11] However, the adsorption capacities of the raw biochars for heavy metals are usually lower due to their limited surface functional groups and mineral components (CO_3^{2-}, PO_4^{3-}).[12,13] Therefore, modification of biochar with novel structures and surface properties to enhance their capacity for heavy metal removal have been attracted more and more attentions. Recently, considerable research interest has been focused on preparation of biochar-based nano-composites to removal organic and inorganic pollutants by combination the advantages of biochar and nanomaterials.[14–18] In this context, various nanoscale materials, such as iron oxides, manganese oxides, ZnS, ZnO, carbon nanotube, graphene, have been used to modify biochar for enhancing their heavy metal adsorption performance.[19–25] While aiming at reliable preparation of low-cost, environmentally friendly biochar–nanomaterial hybrids to achieve the effective decontamination of heavy metal still remains a challenge.

Calcium carbonate ($CaCO_3$), as one of the most abundant materials in nature, has been explored for heavy metal ions removal greatly. Especially, $CaCO_3$ played an important role in specific adsorption of Cd(II) in paddy soils, and majority of Cd(II) existed in the form of Cd–$CaCO_3$ at most flooding periods for Cd(II) contaminated paddy soil.[26–28] However, natural calcite has only a very low efficiency on Cd(II) adsorption.[29,30] Therefore, various nanostructured $CaCO_3$, including calcite, vaterite, amorphous calcium carbonate, and their hybrids, have been

[a]*Key Laboratory of Urban Pollutant Conversion, Institute of Urban Environment, Chinese Academy of Sciences, Xiamen 361021, China. E-mail: hjcui@iue.ac.cn; mlfu@iue.ac.cn*

[b]*University of Chinese Academy of Sciences, Beijing 100039, China*

† Electronic supplementary information (ESI) available: SEM images of the as-obtained calcite in the absence of SSB, SEM images and elemental mapping of SSB and CMSSB samples before and after Cd(II) adsorption, and dissolution kinetics of calcite and CMSSB samples in water at pH 5.0. See DOI: 10.1039/c7ra00324b

fabricated to removal heavy metal ions with high adsorption capacities.[31–36] Regarding this, in this work, the biochar obtained from sewage sludge was modified by nanostructured calcite for the first time, and used for the Cd(II) removal. The removal efficiency of Cd(II) and corresponding removal kinetics for the as-obtained hybrids were investigated. The Cd(II) adsorption mechanism on the nanostructured calcite modified biochar was also discussed. This work will provided an alternately low cost, efficient, and environmentally friendly adsorbent for Cd(II) decontamination of polluted water and soils.

Experimental section

Preparation of sewage sludge biochar (SSB)

Sewage sludge samples with a moisture content of 82.31% were used in this study and supplied by a wastewater treatment plant in Xiamen, Fujian province, China. Before the pyrolysis, the sewage sludge was homogeneously agitated and then kept in a polyethylene plastic bucket in refrigerator at 4 °C. The bucket was airtight to protect the sample from oxidation. The wet sewage sludge was dried at 105 °C for at least 24 h in an oven, then the dried sewage sludge was packed in a vertical tube and pyrolysed at 500 °C (higher yield and fix carbon content[37,38]) to form sewage sludge biochar under a nitrogen gas atmosphere.

Calcite modified sewage sludge biochar (CMSSB)

Calcite was prepared by a modified Cai's method.[31] Briefly, 10 mL of 0.1 M $CaCl_2$ solution was quickly mixed with 90 mL of aqueous solution, which contained 0.01 mol of NaOH, 0.005 mol of dimethyl carbonate, 0.004 mol of poly(acrylic acid), and 2.0 g of SSB. The reaction solution was kept under stirring for about 2.5 min at room temperature. The precipitates were separated rapidly by centrifugation and washed using distilled water and anhydrous acetone, respectively. The samples with different $CaCO_3$/SSB ratio (wt/wt) were prepared by adjusting the amount of SSB. The CMSSB sample with 5 wt% $CaCO_3$ shows the best adsorption capacity for Cd(II) (Fig. S1†), and was used for experiments in this study.

Characterizations

XRD was carried out using a Bruker D8 ADVANCE X-ray diffractometer equipped with monochromated Cu Kα radiation (λ = 0.1541 nm) at a tube voltage of 40 kV and a tube current of 30 mA. SEM images were obtained with a Hitachi S-4800 emission scanning electron microscope. A Micrometrics ASAP 2020M + C system was used to measure the surface areas and micropore size distributions of the materials. N_2 isothermal adsorption and desorption experiments were performed at relative pressures (P/P_0) from 10^{-6} to 0.9944 and from 0.9944 to 0.047, respectively. Pore size distribution was constructed by analyzing desorption data points using the BJH method. All Fourier transform infrared (FT-IR) spectra were obtained with a Thermo Scientific Nicolet iS10 spectrophotometer using pellets with KBr powder. Samples were scanned 15 times between 4000 and 400 cm^{-1} at a resolution of 4 cm^{-1}. The thermal degradation of samples was studied with a thermogravimetric analysis (TG, Netzsch TG 209 F3) from 40 to 800 °C with an N_2 flow rate of 30 mL min^{-1} and a heating rate of 10 °C min^{-1}.

Adsorption experiments

Cadmium (Cd) adsorption capacities of SSB and CMSSB materials were evaluated by measuring the time-dependent concentrations of Cd(II) and total Cd(II) in a batch system. To examine the effect of initial Cd(II) concentration on the Cd(II) adsorption by the SSB and CMSSB materials, 0.015 g L^{-1} of SSB or CMSSB were contacted with 0, 0.5, 0.9, 3.7, 5.3, 7.0, 8.5, and 10.0 mg L^{-1} of Cd(II) solution (150 mL) at initial pH 6.0. The suspensions were agitated on a shaker at 250 rpm and 25 °C for 24 h, after which the suspensions were intermittently filtered through a 0.22 μm syringe filter. For the kinetic adsorption study, 0.015 g of SSB or CMSSB materials were mixed with 8.4 mg L^{-1} of Cd(II) solution (150 mL) at initial pH 7.0. At time zero and at selected time intervals thereafter, 5 mL of the suspensions were taken and filtered through a 0.22 μm syringe filter. In the experiment examining the pH edge, 0.015 g of CMSSB samples was mixed with 2.0 mg L^{-1} of Cd(II) solution (150 mL) at initial pHs of 4.5, 5.5, 6.5, 7.5, and 8.5. The suspensions were agitated on a shaker at 250 rpm and 25 °C for 24 h, after which 5 mL of the solutions were intermittently sampled and filtered through a 0.22 μm syringe filter. The residual Cd(II) concentration was measured by ICP-OES. Batch experiments were conducted in three replicate and the results reported are mean values of the experimental data.

Results and discussion

The XRD patterns of the SSB, CMSSB, and calcite samples are shown in Fig. 1. The XRD pattern of SBB revealed the presence of several mineral phases, and quartz (Q), with a strong characteristic peak at 2θ = 26.6°, was the most recognizable crystallographic structure in the samples. A weak characteristic peak of calcite ($CaCO_3$) was observed, indicating that little calcite contained in the SSB samples. In contrast, the intensity of characteristic peak of calcite increased slightly for the CMSSB samples, suggesting that calcite were successfully deposited on

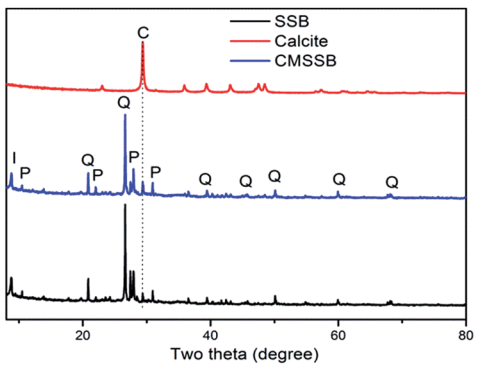

Fig. 1 XRD patterns of calcite, SSB and as-synthesized CMSSB samples (I: illite; P: salt phosphate; Q: quartz; C: calcite).

the surface of the SSB samples. The slight change could be attributed to the small quantity and high dispersion of $CaCO_3$ nanoparticles on the surface of SSB.

The SEM images of SSB and CMSSB samples show that the loading of calcite has slightly effect on the morphology of SSB (Fig. 2), and no obvious calcite nanoparticle aggregates occurred in CMSSB (Fig. S2†). These results indicate that the SSB enhanced the dispersion of $CaCO_3$ nanoparticles and the precipitated calcite mainly existed in the form of nanoparticle on the SSB surface. The Energy dispersive X-ray spectrometry (EDX) spectrum of the SSB and CMSSB samples confirm the increase of Ca element after calcite loading, further validating the formation of calcite nanoparticles on the surface of SSB. The EDX elemental mapping was utilized to further verify the elemental composition of the SSB and CMSSB, as well as the nanoscale spatial uniformity of the element distribution. The Ca element is homogeneously distributed in the CMSSB samples (Fig. S3†), suggesting that loaded calcite is homogeneously distributed on the surface of SSB samples.

The properties of SSB and CMSSB samples are listed in Table 1. Clearly, the Brunauer–Emmett–Teller (BET) surface area of the SSB (28.2 $m^2\ g^{-1}$) is higher than that of the CMSSB sample (25.6 $m^2\ g^{-1}$), but pore size of the SSB (3.1) is lower than that of the CMSSB sample (3.4), In addition, the Ca relative content of the CMSSB (8.8, wt%) was slightly higher than that of the SSB sample (5.8, wt%). The TG analysis presented that the content of $CaCO_3$ nanoparticles in the CMSSB samples is about 5.6 wt% (Fig. S4†), which is close to the given $CaCO_3$/SSB ratio (wt/wt).

The maximum Cd(II) adsorption capacities of the SSB and CMSSB materials were investigated using the equilibrium adsorption isotherms by varying the initial Cd(II) concentrations from 0.05 to 10 mg L^{-1} at pH 6.0. As illustrated in Fig. 3, the amount of Cd(II) adsorbed by the SSB firstly increased with increasing Cd(II) concentrations from 0.05 to 4 mg L^{-1}, and then became to decrease with further increasing Cd(II) concentration over 4 mg L^{-1} (Fig. 3). A similar phenomenon for Cd(II) adsorption on the biochar derived from municipal sewage sludge has also been observed in ref. 37 and 39. By comparison, the sorption amount of Cd(II) continuously increased with increasing the concentration of Cd(II) from 0.05 to 10 mg L^{-1} for CMSSB. Moreover, both the SSB and CMSSB materials are able to reduce the equilibrium Cd(II) concentration to trace levels in the low concentration region (<1 mg L^{-1}). At higher initial Cd(II) concentrations (>1 mg L^{-1}), however, these two materials show different adsorption behaviours, with Cd(II) adsorption capacity of CMSSB being much higher than that of SSB samples. Both Freundlich and Langmuir models are employed to further analyze the Cd(II) adsorption data for CMSSB materials. The equations were as follows:

$$Q_e = K_f \times C_e^{1/n} \quad (1)$$

$$Q_e = b \times Q_m/(1 + b \times C_e) \quad (2)$$

where Q_e is the amount adsorbed per unit weight of sorbent at equilibrium (mg g^{-1}); C_e is the equilibrium concentration (mg L^{-1}), K_f is the Freundlich adsorption constant related to the Cd(II) adsorption capacity of the adsorbent ((mg g^{-1}) (L $mg^{-1})^{1/n}$), and $1/n$ is the adsorption intensity, which indicates the favorability of adsorption. In addition, Q_m is the sorption capacity (mg g^{-1}) and b is the affinity coefficient (L mg^{-1}). According to the value of regression coefficients (R^2), the Langmuir isotherm model describes well the adsorption behavior of Cd(II) on the CMSSB (R^2 = 0.996), indicating that the monolayer adsorption was involved in the Cd(II) removal process by CMSSB.[35] The maximum Cd(II) adsorption capacity based on the Langmuir model is 36.5 mg g^{-1} for CMSSB, which is nearly three times higher than that of

Table 1 Selected characterization of the SSB and CMSSB samples

Adsorbent	BET ($m^2\ g^{-1}$)	Pore size (nm)	Relative content of elements	
			Ca (wt%)	Cd (wt%)
SSB	28.2	3.1	5.8	1.7
CMSSB	25.6	3.4	8.8	1.1

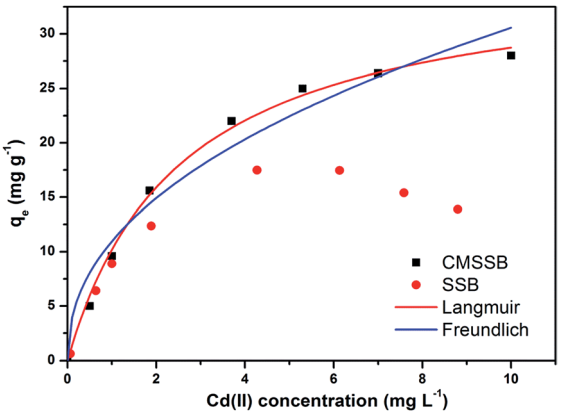

Fig. 3 Adsorption isotherms of Cd(II) on SSB and CMSSB samples (dose of adsorbents, 0.1 g L^{-1}, initial solution pH 6.0).

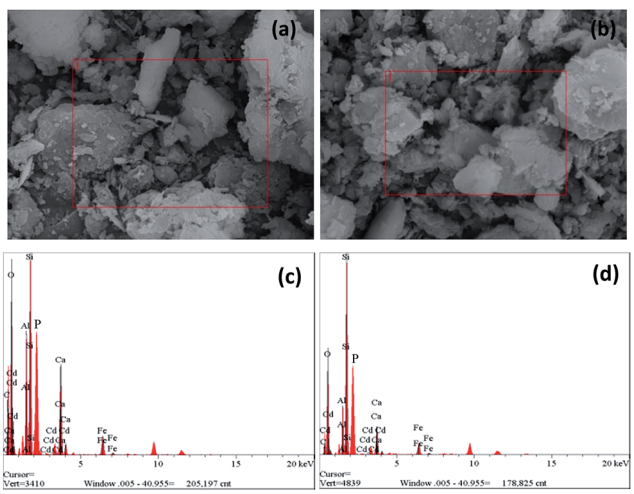

Fig. 2 SEM images and EDX spectra of the SSB (a and c) and CMSSB (b and d) samples.

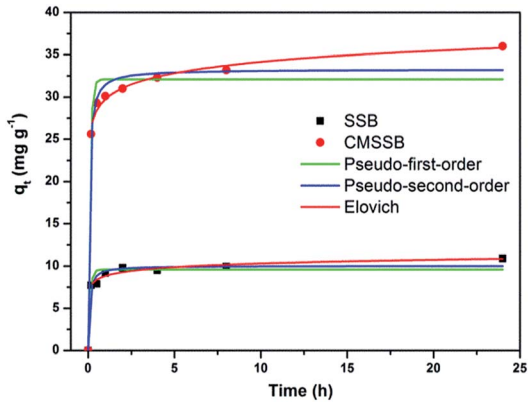

Fig. 4 Adsorption kinetics of Cd(II) onto SSB and CMSSB materials: adsorbent dose, 0.1 g L^{-1}; Cd(II) concentration, 8.4 mg L^{-1}; initial pH 7.0.

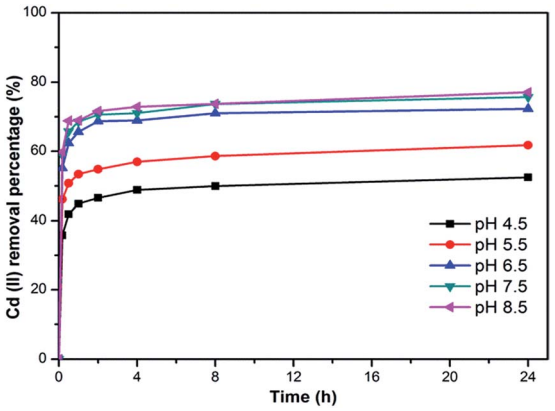

Fig. 5 Effect of the initial solution pH on Cd(II) removal by CMSSB: adsorbent dose, 0.1 g L^{-1}; initial Cd(II) concentration, 2.0 mg L^{-1}.

pristine SSB. Therefore, a small amount of calcite nanoparticles (calcite/SSB = 5 wt%) modification has greatly enhanced the adsorption capacity of Cd(II) compared to the raw sewage sludge biochar.

The time needed for Cd(II) removal using adsorbents is of considerable importance for the possible practical application. The time-dependent Cd(II) adsorption kinetics by the SSB and CMSSB materials are presented Fig. 4. It is apparent that most of Cd(II) could be rapidly adsorbed onto the SSB and CMSSB (Fig. 4). Over 80% of the Cd(II) adsorption capacity was reached within 10 min, and then Cd(II) adsorption increased steadily to reach equilibrium in about 24 h. This slow adsorption rate following initially rapid adsorption of heavy metals on $CaCO_3$ has also been observed previously.[31,35] In order to investigate the mechanism of adsorption and potential rate-controlling steps, the pseudo-first-order, pseudo-second-order, and Elovich equation kinetic models have been employed to fit the experimental data, and the kinetic parameters for Cd(II) adsorption are listed in Table S1.† Compared with R^2 values, kinetics data for the adsorption of Cd(II) from aqueous solution were in best agreement with the Elovich equation. The validity of the Elovich equation suggests that Cd(II) adsorption on the SSB and CMSSB materials is a chemical adsorption on highly heterogeneous adsorbents and chemisorption mechanism is likely rate-controlling in the processes. The α value of CMSSB is much higher than that of SSB (see Table S1†), and the β shows the opposite trend, indicating that the initial adsorption rate of CMSSB is faster than that of SSB materials. Thus, the rate of Cd(II) chemisorption on SSB can be increased with the presence of calcite nanoparticles (CMSSB).

The initial solution pH is one of the most important parameters affecting heavy metal sorption process on $CaCO_3$ and biochar surfaces.[35,40] To explore the effect of solution pH on the adsorption of Cd(II) onto CMSSB, the sorption studies were carried out at pH values adjusted from 4.5 to 8.5. As presented in Fig. 5, the removal efficiency of Cd(II) by CMSSB depends mainly on the pH of the aqueous solutions, and the Cd(II) adsorption increases with increased solution pH, which can also be observed on the single component $CaCO_3$ and biochar samples.[31,37] When the pH is low (pH < 5.5), the adsorption capacities of Cd(II) were low due to the dissolution of calcite and the electrostatic repulsion.[41,42] A remarkable release of Ca(II) has been detected in the single calcite or CMSSB suspension at pH 5.0 (Fig. S5†). Meanwhile, the species of surface functional groups on biochar–calcite were protonized with positively charged surface, resulting in competition between H^+ and Cd(II) or Ca(II) and Cd(II) for occupancy of the binding sites.[42] With increasing pH values (pH > 5.5), more calcite nanoparticles could exist in the solutions, causing a greater ion-exchange reaction between Cd(II) and Ca(II) at the surface of CMSSB. In addition, the surface charges of biochar–calcite became more negative, further promoting the Cd(II) sequestration and eventually resulting in high Cd(II) removal efficiency.[12]

Many researchers have investigated heavy metal cation adsorption mechanisms on calcite and SSB materials, and the ion exchange, electrostatic attraction, surface complexation, physical sorption, and precipitation have been suggested by several researchers.[8,12,43–46] To explore the Cd(II) removal mechanism, the calcite, SSB, original and Cd(II)-loaded CMSSB samples were scanned by FT-IR, respectively. After Cd(II) adsorption on CMSSB, the band intensities at 1427 and 879 cm^{-1}, which corresponded to calcite, clearly decreased (Fig. 6a). The degrease of the two peaks was attributed to ion exchange or surface precipitation of metal-(hydro)carbonates. Meanwhile, other adsorption band intensities did not change remarkably after Cd(II) adsorption (Fig. 6a). These results indicate that calcite play a key role in Cd(II) adsorption. A

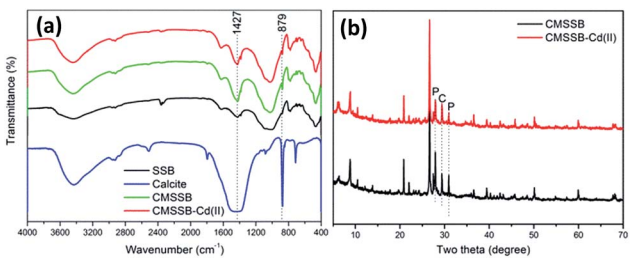

Fig. 6 (a) FT-IR spectra of calcite, SSB, original and Cd(II)-loaded CMSSB; (b) XRD patterns of the original and Cd(II)-loaded CMSSB.

precipitation transformation has been proposed for heavy metal adsorption on $CaCO_3$ materials.[31,32,41,42] To further confirm the contribution of the chemical precipitation for Cd(II) sorption, the original and Cd(II)-loaded CMSSB were analyzed by XRD. As shown in Fig. 6b, the characterization diffraction peaks in the XRD pattern of Cd(II)-loaded CMSSB is similar to that of the initial CMSSB, suggesting that no significant crystal structure precipitates were formed during the Cd(II) sorption on CMSSB. In contrast, the intensity of phosphate decreased after Cd(II) adsorption, indicating that Cd(II) precipitates with phosphate was also involved in Cd(II) adsorption reaction. Based on the ICP and FT-IR analysis (Fig. 4), it was concluded that Cd(II) mainly adsorbed on calcite nanoparticles in CMSSB. Meanwhile, the SEM-EDX elemental mapping of Cd(II) loaded CMSSB samples shown a close association of Cd with Ca (Fig. S6†), further suggesting that Cd(II) adsorption or precipitation occurred on the surface of calcite nanoparticles.

Conclusions

The nanostructured calcite modified sewage sludge biochar materials have been successfully prepared through a simple precipitate method. The loaded calcite nanoparticles significantly improve the adsorption performance of the biochars for Cd(II). The substantially lower cost and higher efficiency of this adsorbent, become the main advantages of this composite. These preliminary results demonstrate that nanostructured calcite modified biochars will have a great potential application for heavy metal decontamination of polluted water.

Acknowledgements

This work was financially supported by National Natural Science Foundation of China (No. 41371244, and 51478449) and China-Japanese Research Cooperative Program (2016YFE0118000).

Notes and references

1 L. Järup and A. Åkesson, *Toxicol. Appl. Pharmacol.*, 2009, **238**, 201–208.
2 Y. Hu, H. Cheng and S. Tao, *Environ. Int.*, 2016, **92–93**, 515–532.
3 F. Fu and Q. Wang, *J. Environ. Manage.*, 2011, **92**, 407–418.
4 N. Bolan, A. Kunhikrishnan, R. Thangarajan, J. Kumpiene, J. Park, T. Makino, M. B. Kirkham and K. Scheckel, *J. Hazard. Mater.*, 2014, **266**, 141–166.
5 X. Dou, D. Chen, Y. Hu, Y. Feng and X. Dai, *J. Hazard. Mater.*, 2017, **321**, 132–145.
6 M. Ahmad, A. U. Rajapaksha, J. E. Lim, M. Zhang, N. Bolan, D. Mohan, M. Vithanage, S. S. Lee and Y. S. Ok, *Chemosphere*, 2014, **99**, 19–33.
7 A. Bogusz, P. Oleszczuk and R. Dobrowolski, *Bioresour. Technol.*, 2015, **196**, 540–549.
8 M. I. Inyang, B. Gao, Y. Yao, Y. Xue, A. Zimmerman, A. Mosa, P. Pullammanappallil, Y. S. Ok and X. Cao, *Crit. Rev. Environ. Sci. Technol.*, 2016, **46**, 406–433.
9 H.-J. Cui, M. K. Wang, M.-L. Fu and E. Ci, *J. Soils Sediments*, 2011, **11**, 1135.
10 C. J. Atkinson, J. D. Fitzgerald and N. A. Hipps, *Plant Soil*, 2010, **337**, 1–18.
11 D. Mohan, A. Sarswat, Y. S. Ok and C. U. Pittman Jr, *Bioresour. Technol.*, 2014, **160**, 191–202.
12 X. Tan, Y. Liu, G. Zeng, X. Wang, X. Hu, Y. Gu and Z. Yang, *Chemosphere*, 2015, **125**, 70–85.
13 M. B. Ahmed, J. L. Zhou, H. H. Ngo, W. Guo and M. Chen, *Bioresour. Technol.*, 2016, **214**, 836–851.
14 Z. Han, B. Sani, W. Mrozik, M. Obst, B. Beckingham, H. K. Karapanagioti and D. Werner, *Water Res.*, 2015, **70**, 394–403.
15 K.-W. Jung and K.-H. Ahn, *Bioresour. Technol.*, 2016, **200**, 1029–1032.
16 J. Yan, L. Han, W. Gao, S. Xue and M. Chen, *Bioresour. Technol.*, 2015, **175**, 269–274.
17 P. Devi and A. K. Saroha, *Bioresour. Technol.*, 2014, **169**, 525–531.
18 X. Hu, Z. Ding, A. R. Zimmerman, S. Wang and B. Gao, *Water Res.*, 2015, **68**, 206–216.
19 Z. Song, F. Lian, Z. Yu, L. Zhu, B. Xing and W. Qiu, *Chem. Eng. J.*, 2014, **242**, 36–42.
20 J. Tang, H. Lv, Y. Gong and Y. Huang, *Bioresour. Technol.*, 2015, **196**, 355–363.
21 M. Inyang, B. Gao, A. Zimmerman, Y. Zhou and X. Cao, *Environ. Sci. Pollut. Res.*, 2015, **22**, 1868–1876.
22 L. Yan, L. Kong, Z. Qu, L. Li and G. Shen, *ACS Sustainable Chem. Eng.*, 2015, **3**, 125–132.
23 S. Wang, B. Gao, Y. Li, A. Mosa, A. R. Zimmerman, L. Q. Ma, W. G. Harris and K. W. Migliaccio, *Bioresour. Technol.*, 2015, **181**, 13–17.
24 C. Gan, Y. Liu, X. Tan, S. Wang, G. Zeng, B. Zheng, T. Li, Z. Jiang and W. Liu, *RSC Adv.*, 2015, **5**, 35107–35115.
25 M. Zhang, B. Gao, S. Varnoosfaderani, A. Hebard, Y. Yao and M. Inyang, *Bioresour. Technol.*, 2013, **130**, 457–462.
26 X. Zhao, T. Jiang and B. Du, *Chemosphere*, 2014, **99**, 41–48.
27 S. Khaokaew, R. L. Chaney, G. Landrot, M. Ginder-Vogel and D. L. Sparks, *Environ. Sci. Technol.*, 2011, **45**, 4249–4255.
28 P. Kosolsaksakul, J. G. Farmer, I. W. Oliver and M. C. Graham, *Environ. Pollut.*, 2014, **187**, 153–161.
29 A. Martin-Garin, P. Van Cappellen and L. Charlet, *Geochim. Cosmochim. Acta*, 2003, **67**, 2763–2774.
30 I. A. M. Ahmed, N. M. J. Crout and S. D. Young, *Geochim. Cosmochim. Acta*, 2008, **72**, 1498–1512.
31 G.-B. Cai, G.-X. Zhao, X.-K. Wang and S.-H. Yu, *J. Phys. Chem. C*, 2010, **114**, 12948–12954.
32 C. Li, Z.-j. Qian, C. Zhou, W. Su, P. Hong, S. Liu, L. He, Z. Chen and H. Ji, *RSC Adv.*, 2014, **4**, 47848–47852.
33 Z. Liu, Q. Shen, Q. Zhang, L. Bian, Y. Liu, B. Yuan, X. Pan and F. Jiang, *J. Mater. Sci.*, 2014, **49**, 5334–5344.
34 A. M. Lopez_Marzo, J. Pons and A. Merkoci, *J. Mater. Chem. A*, 2014, **2**, 8766–8772.
35 M. S. Islam, W. S. Choi, B. Nam, C. Yoon and H.-J. Lee, *Chem. Eng. J.*, 2017, **307**, 208–219.
36 J. Zhang, B. Yao, H. Ping, Z. Fu, Y. Li, W. Wang, H. Wang, Y. Wang, J. Zhang and F. Zhang, *RSC Adv.*, 2016, **6**, 472–480.

37 T. Chen, Y. Zhang, H. Wang, W. Lu, Z. Zhou, Y. Zhang and L. Ren, *Bioresour. Technol.*, 2014, **164**, 47–54.
38 H. Yuan, T. Lu, H. Huang, D. Zhao, N. Kobayashi and Y. Chen, *J. Anal. Appl. Pyrolysis*, 2015, **112**, 284–289.
39 T. Chen, Z. Zhou, R. Han, R. Meng, H. Wang and W. Lu, *Chemosphere*, 2015, **134**, 286–293.
40 L. Qian, W. Zhang, J. Yan, L. Han, W. Gao, R. Liu and M. Chen, *Bioresour. Technol.*, 2016, **206**, 217–224.
41 X. Ma, L. Li, L. Yang, C. Su, K. Wang, S. Yuan and J. Zhou, *J. Hazard. Mater.*, 2012, **209–210**, 467–477.
42 X. Ma, W. Cui, L. Yang, Y. Yang, H. Chen and K. Wang, *Bioresour. Technol.*, 2015, **185**, 70–78.
43 X. Cui, S. Fang, Y. Yao, T. Li, Q. Ni, X. Yang and Z. He, *Sci. Total Environ.*, 2016, **562**, 517–525.
44 X. Cao, L. Ma, B. Gao and W. Harris, *Environ. Sci. Technol.*, 2009, **43**, 3285–3291.
45 O. R. Harvey, B. E. Herbert, R. D. Rhue and L.-J. Kuo, *Environ. Sci. Technol.*, 2011, **45**, 5550–5556.
46 H. Lu, W. Zhang, Y. Yang, X. Huang, S. Wang and R. Qiu, *Water Res.*, 2012, **46**, 854–862.